





Dynamics of large samples of repulsive Fermi gases at nonzero temperatures

Jarosław Ryszkiewicz , Mirosław Brewczyk , and Tomasz Karpiuk 
Wydział Fizyki, Uniwersytet w Białymstoku, ul. K. Ciołkowskiego 1L, 15-245 Białystok, Poland

 (Received 16 September 2021; revised 3 January 2022; accepted 27 January 2022; published 14 February 2022)

We develop a model of a binary fermionic mixture, consisting of a large number of atoms, applicable at nonzero temperatures, in the normal phase. We use this approach to study the dynamics of degenerate Fermi systems under various perturbations. For example, we analyze the spin-dipole oscillations of a two-component fermionic mixture, demonstrating that the ferromagnetic phase shows up at a stronger repulsion between components while the temperature rises. We study as well the radial oscillations of weakly interacting repulsive Fermi gases. We obtain a good agreement with experimental data when available. Otherwise, we compare our results with the outcome of the Hartree-Fock orbital calculations done for a system with a small number of fermions.

DOI: [10.1103/PhysRevA.105.023315](https://doi.org/10.1103/PhysRevA.105.023315)

I. INTRODUCTION

Systems of ultracold fermionic atoms have been already studied for years, both experimentally and theoretically. Since the first experimental achievement of quantum degeneracy in fermionic potassium gas [1], followed by successful attempts to cool other elements [2–5], the interest in cold fermionic gases has quickly increased, covering a broad range of quantum many-body phenomena including thermodynamic and transport-related effects at unitarity [6–8], correlations, in particular in optical lattices [9–16] or near Feshbach resonances [17–19], strongly interacting gases in lower dimensions [20–25], or dipolar gases [26–29].

In particular, the dynamics of fermionic gases has been thoroughly investigated. The measurement of collective mode frequencies and damping rates as a function of temperature supplied evidence for the superfluid behavior of a Fermi gas [30], while an observation of a vortex lattice [31] provided direct verification of superfluidity. By exciting hydrodynamic modes, such as collective oscillations [30,32,33], sound [34], or rotational modes [35], the transport properties of a unitary Fermi gas have been experimentally determined. A careful analysis of compression, quadrupole, and scissor modes in the unitarity limit in the range of temperatures above the critical temperature for superfluidity has been performed in Ref. [36] and revealed a transition from hydrodynamic to collisionless behavior with an increase of temperature. Recently, oscillations of a repulsive binary fermionic mixture [37,38], initially phase separated by a domain wall, were studied experimentally in connection with the long-standing problem of Stoner instability [39].

In this paper we investigate the finite-temperature dynamics of Fermi-Fermi mixtures by using a density-functional-like description. To derive the equations of motion we start by introducing the semiclassical distribution function for fermions. Then we evoke the Kohn and Sham [40] way of treating a nonzero temperature case within the density-functional methods and replace the local kinetic energy expression by the one corresponding to free energy. Next, we switch to the

quantum hydrodynamic description [41] of the system, apply the inverse Madelung transformation [42–44], and follow the Dirac prescription [45] to get the desired equations.

The paper is then organized as follows. First, we present the model of a two-component Fermi gas in the normal phase capable of retrieving the dynamics when the number of atoms is large (Sec. II). To prove the effectiveness of our model we compare numerical results to experimental data on the dynamics of fermionic systems in the case of spin-dipole modes [38] (Sec. III) and to the outcome of the Hartree-Fock orbital calculations in the case of radial oscillations of a weakly interacting repulsive Fermi gas (Sec. IV). We conclude in Sec. V.

II. EQUATIONS OF MOTION

A simple description of a one-component gas in terms of a semiclassical distribution function $f_{\mathbf{p}}(\mathbf{r})$ assumes that $f_{\mathbf{p}}(\mathbf{r})d\mathbf{r}d\mathbf{p}/(2\pi\hbar)^3$ gives the mean number of particles in the phase-space volume element $d\mathbf{r}d\mathbf{p}$. At equilibrium, at a given temperature T and a chemical potential μ , one has for a degenerate Fermi gas

$$f_{\mathbf{p}}(\mathbf{r}) = \frac{1}{e^{[\varepsilon_{\mathbf{p}}(\mathbf{r}) - \mu]/k_B T} + 1}, \quad (1)$$

with $\varepsilon_{\mathbf{p}}(\mathbf{r})$ being the particle energy at position \mathbf{r} . For a single-component ideal Fermi gas in a trap this energy becomes

$$\varepsilon_{\mathbf{p}}(\mathbf{r}) = \frac{\mathbf{p}^2}{2m} + V_{\text{tr}}(\mathbf{r}). \quad (2)$$

The density of particles is obtained by integrating the distribution function over all momenta $n(\mathbf{r}) \sim \int f_{\mathbf{p}}(\mathbf{r})d\mathbf{p}$. Other kinds of energies can be added to Eq. (2), in particular the one related to the Weizsäcker correction $E_W = \xi(T)(\hbar^2/2m) \int [\nabla \sqrt{n(\mathbf{r})}]^2 d\mathbf{r}$, with a weakly temperature-dependent coefficient $\xi(T)$ [46]. Now, when the other fermionic component comes to the scene, the interaction energy has to be included as well. Assuming the intercomponent interactions only depend on densities $V_{\text{int}}(n_+, n_-)$ (hereafter the components are distinguished by the indices “+” and

“—”), Eq. (2) becomes

$$\varepsilon_{\mathbf{p}}(\mathbf{r}) = \frac{\mathbf{p}^2}{2m} + V_{\text{tr}}(\mathbf{r}) + \frac{\delta E_W^+}{\delta n_+} + \frac{\delta V_{\text{int}}}{\delta n_+}. \quad (3)$$

The density of particles of the + component is calculated as

$$\begin{aligned} n_+(\mathbf{r}) &= \int \frac{1}{e^{[\varepsilon_{\mathbf{p}}(\mathbf{r}) - \mu_+]/k_B T} + 1} \frac{d\mathbf{p}}{(2\pi\hbar)^3} \\ &= \frac{1}{\lambda^3} f_{3/2}(z_+), \end{aligned} \quad (4)$$

and the energy density related to the local motion as

$$\begin{aligned} \varepsilon_+(\mathbf{r}) &= \int \frac{\mathbf{p}^2/2m}{e^{[\varepsilon_{\mathbf{p}}(\mathbf{r}) - \mu_+]/k_B T} + 1} \frac{d\mathbf{p}}{(2\pi\hbar)^3} \\ &= \frac{3}{2} \frac{k_B T}{\lambda^3} f_{5/2}(z_+), \end{aligned} \quad (5)$$

where k_B is the Boltzmann constant, $\lambda = \sqrt{2\pi\hbar^2/mk_B T}$ is the thermal wavelength, and $f_{3/2}(z)$ and $f_{5/2}(z)$ are the standard functions for fermions [47]. The “extended fugacity” equals

$$z_+(\mathbf{r}) = e^{(\mu_+ - V_{\text{tr}}(\mathbf{r}) - \delta E_W^+/\delta n_+ - \delta V_{\text{int}}/\delta n_+)/k_B T}. \quad (6)$$

The chemical potential μ_+ is determined by the normalization condition $N_+ = \int n_+(\mathbf{r})d\mathbf{r}$.

According to the Kohn and Sham proposition [40] on a generalization of the density-functional formalism to the finite-temperature case, for a further analysis the energy of the system should be replaced by its free energy, whose density is

$$f_+(\mathbf{r}) = \frac{k_B T}{\lambda^3} [(\ln z_+)f_{3/2}(z_+) - f_{5/2}(z_+)]. \quad (7)$$

Additionally, in a dynamical case the energy functional has to be modified by adding the energy of a macroscopic flow. Then the part of the functional related to the + component, which is minimized to get the equations underlying the system’s dynamics, becomes

$$\begin{aligned} F_+(n_+, \mathbf{v}_+) &= \int f_+(\mathbf{r})d\mathbf{r} + \int n_+ \frac{1}{2} m \mathbf{v}_+^2 d\mathbf{r} \\ &\quad + \int V_{\text{tr}}(\mathbf{r})n_+ d\mathbf{r} + E_W + V_{\text{int}}. \end{aligned} \quad (8)$$

Here, $\mathbf{v}_+(\mathbf{r})$ is the velocity field of a macroscopic flow of the + fermionic component and the second term on the right-hand side represents the energy of such motion.

Now we introduce the pseudowave function $\psi_+(\mathbf{r})$ ($n_+ = |\psi_+|^2$) for the + component in such a way that

$$\frac{\hbar^2}{2m} (\nabla \psi_+^*) (\nabla \psi_+) = \frac{\hbar^2}{2m} (\nabla |\psi_+|)^2 + n_+ \frac{1}{2} m \mathbf{v}_+^2. \quad (9)$$

The functional Eq. (8) is then transformed to

$$\begin{aligned} F_+(\psi_+, \nabla \psi_+) &= \int f_+(\mathbf{r})d\mathbf{r} + \int \left(-\frac{\hbar^2}{2m} \psi_+^* \nabla^2 \psi_+ \right) d\mathbf{r} \\ &\quad - \frac{\hbar^2}{2m} \int (\nabla |\psi_+|)^2 d\mathbf{r} \\ &\quad + \int V_{\text{tr}}(\mathbf{r})n_+ d\mathbf{r} + E_W + V_{\text{int}}. \end{aligned} \quad (10)$$

A similar functional applies to the second component. The equations of motion are

$$i\hbar \frac{\partial}{\partial t} \psi_{\pm}(\mathbf{r}, t) = \frac{\delta}{\delta \psi_{\pm}^*} F_{\pm}[\psi_{\pm}, \nabla \psi_{\pm}]. \quad (11)$$

Since

$$\frac{\delta}{\delta n_{\pm}} \int f_{\pm}(\mathbf{r})d\mathbf{r} = k_B T \ln z_{\pm}, \quad (12)$$

the equations of motion become

$$\begin{aligned} i\hbar \frac{\partial \psi_{\pm}}{\partial t} &= \left(-\frac{\hbar^2}{2m} \nabla^2 + \frac{\hbar^2}{2m} \frac{\nabla^2 |\psi_{\pm}|}{|\psi_{\pm}|} + k_B T \ln z_{\pm} \right. \\ &\quad \left. + V_{\text{tr}} - \xi(T) \frac{\hbar^2}{2m} \frac{\nabla^2 \sqrt{n_{\pm}}}{\sqrt{n_{\pm}}} + \frac{\delta V_{\text{int}}}{\delta n_{\pm}} \right) \psi_{\pm}. \end{aligned} \quad (13)$$

While solving Eqs. (13), the extended fugacities $z_{\pm}(\mathbf{r})$ are found from the self-consistency condition $f_{3/2}(z_{\pm}) = \lambda^3 n_{\pm}$ [Eq. (4)] with $n_{\pm} = |\psi_{\pm}|^2$. The Weizsäcker correction (the one before the last one) becomes less important when the number of atoms increases.

III. SPIN-DIPOLE OSCILLATIONS

We first examine our model in the case of an experiment on spin-dipole oscillations of repulsive two-component fermionic mixtures [38]. This experiment was aimed to prove the existence of the phase transition from the paramagnetic to ferromagnetic phase in a system of a two-component short-range repulsive Fermi gas, i.e., to resolve the long-standing hypothesis of itinerant ferromagnetism posed by Stoner [39]. It was predicted in Ref. [39] that nonlocalized electrons get into a ferromagnetic state when short-range repulsion between opposite spin electrons becomes large enough to beat the Fermi pressure.

To minimize the effect of the pairing phenomenon [18,19], in the experiment of Ref. [38] a mixture of ${}^6\text{Li}$ atoms was prepared in a special state, in which both components were spatially separated. It was realized in two steps. First, the components held in a prolate harmonic trap were spatially separated by using a magnetic field gradient. Next, when the overlap of two components was small enough, the optical repulsive barrier separating clouds was switched on and the magnetic field gradient was turned off. Then the optical barrier was suddenly removed and the spin dynamics, i.e., oscillations of centers of mass of each component, was studied. Both frequencies and damping rates were measured, which demonstrated the existence of a critical repulsion between components. For weak repulsion the effect of softening of the spin-dipole mode was observed, i.e., the frequency of the oscillations was continuously decreasing with the strength of a repulsion. Simultaneously, both atomic clouds were passing through each other. For stronger repulsion, however, qualitatively different behavior was found. Two atomic clouds started to bounce off each other with a frequency higher than the axial trap frequency.

To model the experiment of Ref. [38] with Eqs. (13), we first obtain the initial state of a two-component Fermi gas by solving Eqs. (13) the by imaginary-time technique [48] in the presence of a cigar-shaped harmonic trap with radial

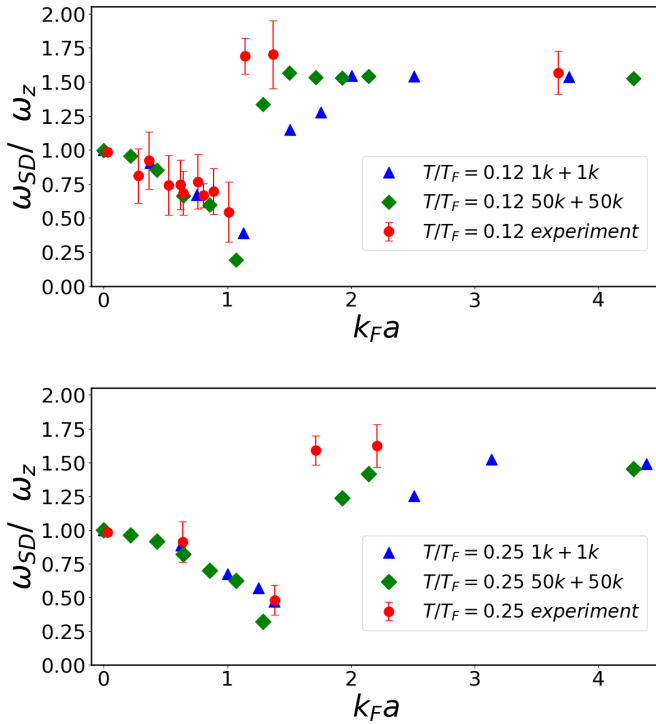


FIG. 1. Frequencies of the spin-dipole mode of a repulsive two-component Fermi gas plotted as a function of $k_F a$ for the temperatures $T/T_F = 0.12$ (upper frame) and $T/T_F = 0.25$ (lower frame)—a comparison with the experiment of Ref. [38]. Simulations were performed for a system with the number of atoms equal to $N/2 = 50\,000$ (as in the experiment), where the Weizsäcker correction in Eq. (13) can be safely neglected, and $N/2 = 1000$.

and axial frequencies equal to $\omega_{\perp} = 2\pi \times 265$ Hz and $\omega_z = 2\pi \times 21$ Hz, respectively, and in the presence of a repulsive optical barrier. Then we remove the barrier and monitor the dynamics of the system by calculating the relative distance $d(t)$ between the centers of two spin clouds. Analyzing $d(t)$ as a function of time we extract both the frequency and the damping rate of the mode (see Ref. [49] for details).

To get an agreement with the experimental data we must include in the model the many-body correlations due to interactions. This can be achieved by renormalizing the coupling constant in the two-body contact potential [44,49,50]. For a uniform system, it is done in a way to get a correct low-density expansion, in the parameter $\tilde{k}_F a$, of an energy of a two-component Fermi gas [see Eq. (3) in Ref. [49]]. Here, \tilde{k}_F is the Fermi wave number and a is the s -wave scattering length. For a trapped gas a local density approximation is used. In the mean-field approximation the interaction energy density is gn_+n_- , with $g = 4\pi\hbar^2 a/m$, and the term $\delta V_{\text{int}}/\delta n_{\pm} = gn_{\mp}$ appears in Eqs. (13). After renormalization, the gn_{\pm} term is replaced by $gn_{\pm} + A(4/3 n_{\mp}^{1/3} n_{\pm} + n_{\pm}^{4/3}) + B(5/3 n_{\mp}^{2/3} n_{\pm} + n_{\pm}^{5/3})$ with $A = 3ga(6\pi^2)^{1/3}(11 - 2 \ln 2)/35\pi$ and $B = 3ga^2(6\pi^2)^{2/3}\pi/4 \times 0.23$ [44].

In Fig. 1 we show the numerical results for frequencies of the spin-dipole mode for two temperatures studied experimentally in Ref. [38] (see Fig. 2). In the upper frame an additional experimental point (most right) is included [see Fig. 3(c) in Ref. [38]]. Simulations were performed for the system

both with the number of atoms as in the experiment (50 000 atoms in each component) and much smaller ($N/2 = 1000$). Figure 1 proves an overall agreement between the numerics and experimental data. Our calculations reveal a softening of the spin-dipole mode followed by a transition from the paramagnetic to ferromagnetic phase. The hydrodynamic model we developed gives the correct value of $k_F a$ [here, $k_F = (24N)^{1/6}/(\hbar/m\bar{\omega})^{1/2}$, where $\bar{\omega}$ is the geometric mean of trap frequencies in all directions] at which this transition occurs. It is already well understood that at zero temperature the softening phenomenon depends solely on the combination $k_F a$ [51]. Our simulations support this observation also for nonzero temperatures (see Fig. 1). According to Stoner's model the transition to the ferromagnetic phase depends on $k_F a$ only as well, which again is exhibited by our simulations.

Above the critical value of $k_F a$ both components stop to penetrate each other and oscillate with frequencies smaller than twice the axial trap frequency, in agreement with experiment. Numerical results seem to be consistent for the two considered numbers of atoms. Our observation is, however, that the size of the intermediate regime (the one between the paramagnetic and ferromagnetic regimes) differs depending on the number of atoms in the sample. For larger systems the large ($k_F a$) value of the oscillation frequency is reached faster, i.e., for smaller $k_F a$. This can be understood as follows. For small samples ($N = 1000$ in our case) even after crossing the critical value of $k_F a$ we can still observe the gas transmission through the intercomponent interface on the perimeter. Hence, in the intermediate regime the flow is partially still miscible. The full transition into the immiscible regime [i.e., when the oscillation frequency takes its large ($k_F a$) value] is then shifted to stronger interactions. This transition occurs faster (in terms of $k_F a$) for larger systems. It happens because, first, the damping rates for spin-dipole oscillations are high for the values of repulsion strengths $k_F a$ close to the critical one (see Fig. 3 in Ref. [49]), and, second, these rates are bigger for systems with a larger number of atoms. Since damping rates decrease with temperature, the intermediate region broadens with temperature.

Figure 2 summarizes the hydrodynamic calculations performed for smaller atomic samples (Fig. 1 demonstrates that the transition to the ferromagnetic phase occurs actually at the same value of $k_F a$, independently of the number of atoms). In the upper frame we show the frequencies of the spin-dipole mode for two additional temperatures, $T/T_F = 0.4$ and $T/T_F = 0.53$, for a system consisting of 1000 atoms in each component. These temperatures were studied in Ref. [38], although in a different way—not by following the spin-dipole oscillations but by analyzing the stability of the initially created spin domains. The lower frame is the phase diagram, which gathers the results corresponding to the transition between the paramagnetic and ferromagnetic phases. This diagram shows the critical value of $k_F a$ as a function of temperature. The experimental data are marked as red crosses, taken from Ref. [38] [see Fig. 3(d) therein], while numerical results are shown as blue bullets. The solid line is a power-law fit to the numerical points and separates the paramagnetic and ferromagnetic phases. At a given value of $k_F a$ the ferromagnetic phase is entered while the system's temperature is decreased, in qualitative agreement with Stoner's model

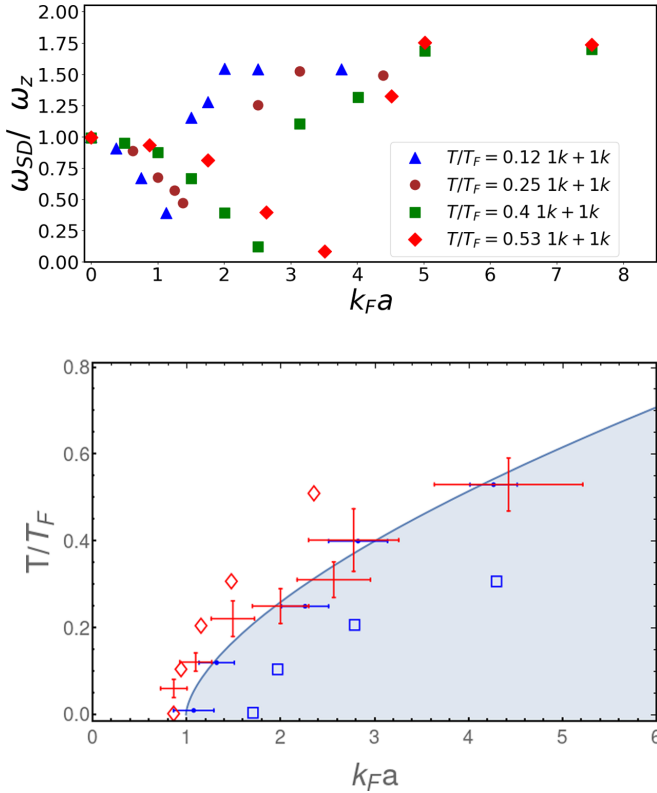


FIG. 2. Upper frame: Frequencies of the spin-dipole mode of a repulsive two-component Fermi gas plotted as a function of $k_F a$ for different temperatures, up to $T/T_F = 0.53$. Lower frame: Phase diagram showing the critical value of the repulsive interaction strength at a given temperature. The red crosses are the experimental data taken from Ref. [38] [see Fig. 3(d) therein], while the blue bullets come from numerics. The solid line, which is a power-law fit to the numerical points, separates the paramagnetic (white area) from the ferromagnetic (dark area) phase. Blue squares and red diamonds are the predictions of static Stoner's model assuming interactions between atoms are not normalized and are renormalized, respectively.

of itinerant ferromagnetism—the ferromagnetic phase rises when interactions are able to overcome the fermionic quantum pressure, which decreases with decreasing temperature.

To check on a quantitative level our numerical (dynamic) results versus predictions of the original (static) Stoner's model we compare the kinetic energy of the gas to its interaction energy at equilibrium [52]. In the simplest case, i.e., in the mean-field approximation, the interaction energy is $g \int n_+ n_- d\mathbf{r}$ and the above-mentioned comparison reads

$$\frac{3 k_B T}{2 \lambda^3} \int f_{5/2}(z_+) d\mathbf{r} = \frac{4\pi \hbar^2}{m k_F} \left(\int n_+ n_- d\mathbf{r} \right) (k_F a)_{\text{cr}}. \quad (14)$$

The critical value of the repulsive interactions $(k_F a)_{\text{cr}}$ is found assuming equal component densities $n_+ = n_- = f_{3/2}(z_+)/\lambda^3$ normalized to $N_+ = N_- = 1000$ with $z_+ = \exp[(\mu_+ - V_{\text{tr}})/k_B T]$. The critical values $(k_F a)_{\text{cr}}$ as a function of T/T_F are plotted in Fig. 2 (lower frame) as blue squares. At zero temperature $(k_F a)_{\text{cr}} \approx 1.7$, in agreement with our earlier calculations [44] [see Fig. 1(d) therein]. When the interactions between atoms become renormalized, the condition (14) changes into a third degree polynomial equation for the

critical interactions $(k_F a)_{\text{cr}}$. The solutions as a function of T/T_F are shown in Fig. 2 (lower frame) as red diamonds. Now, at zero temperature $(k_F a)_{\text{cr}} \approx 0.9$, in agreement with the experimental data of Ref. [38] at the lowest temperature. The overall behavior of $(k_F a)_{\text{cr}}$ resembles the one determined experimentally and obtained in numerical simulations (both representing the dynamical Stoner effect), especially for lower temperatures.

A note regarding the consistency of presented results with those reported already in Refs. [44,49] is now in order. First, the frequency of the spin-dipole mode in a ferromagnetic phase strongly depends on the geometry of the trapping potential, while a density-functional method is used. In an elongated trap, as in the experiment of Ref. [38], it is about 1.7 (see Fig. 2, upper frame). At zero temperature and in a spherically symmetric trap this frequency approaches a value of twice the trap frequency [44], with a recognizable admixture of the other frequency ($\omega_{\text{SD}}/\omega_z = \sqrt{2}$). On the other hand, within the Hartree-Fock approach the spin-dipole mode frequency in a ferromagnetic phase remains twice the axial frequency, independently of temperature [49]. This probably happens because our treatment of the Hartree-Fock dynamics at nonzero temperatures does not allow for atoms to change between single-particle orbitals during the evolution. In our case only one-particle orbitals change in time during the dynamics, not the populations—populations are chosen by using a Monte Carlo sampling technique, before the barrier separating components is removed (for an approach in which populations are treated on the same way as orbitals, although at equilibrium only, see Ref. [53]).

IV. OSCILLATIONS OF WEAKLY INTERACTING REPULSIVE FERMIONIC MIXTURES

In this section we carry out simulations of the dynamics of a two-component weakly interacting Fermi gas, initially confined in a spherically symmetric trap, after a weak disturbance of the trapping potential. Within a weak-driving regime the system's response can be treated analytically in the range of high temperatures and in the limit of an ideal gas. Here, we are verifying our description of large Fermi systems by studying the monopole oscillations of a Fermi gas for weak repulsive interactions. As in Sec. III, we use a renormalized interaction to describe the two-component weakly interacting Fermi gas.

Both gases are perturbed in phase, i.e., two atomic clouds are first simultaneously being squeezed as an effect of increasing trap frequencies and next the trapping potential is slightly attenuated (by decreasing trap frequencies) to allow the gas to expand. Such a cycle is repeated a few times after which the system starts to oscillate in a trap. In this way the spherically symmetric oscillations are excited. We find the frequencies of such excitations by calculating the width of an atomic cloud $\int d^3 \mathbf{r} r^2 n_{\pm}(\mathbf{r}, t)$ and analyzing its time dependence. We show the frequencies of in-phase monopole modes as a function of temperature in Fig. 3, limiting ourselves only to the paramagnetic range of parameters [54–56]. At zero temperature (open circle data) our results perfectly match those obtained within the time-dependent Hartree-Fock method (see Ref. [54]). In the limit of no interaction between components, the spherically symmetric mode oscillates with

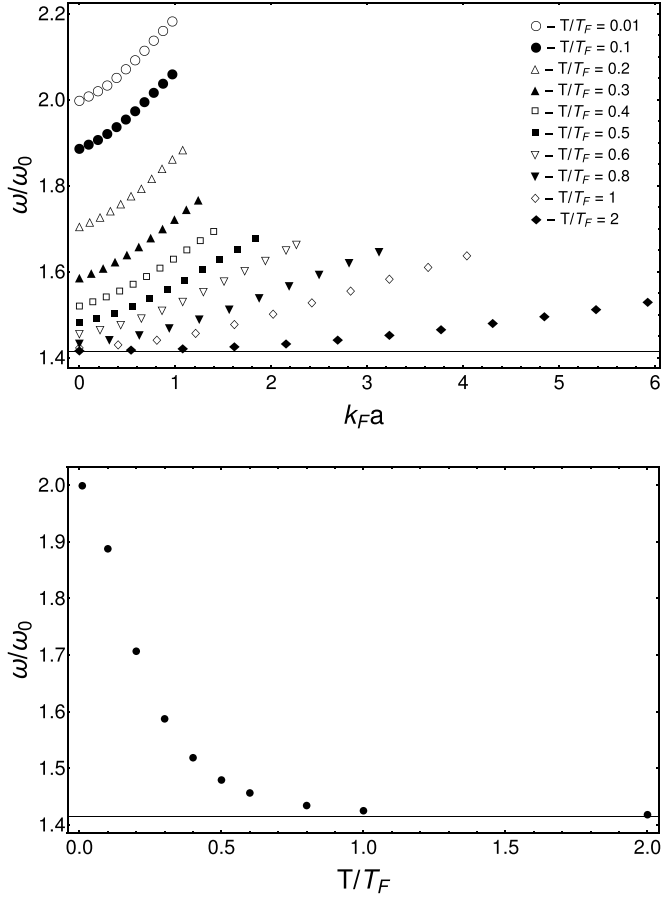


FIG. 3. Upper frame: Frequencies of in-phase monopole modes as a function of temperature. The critical interaction for which the phase separation occurs depends on temperature. Only frequencies of modes excited in the paramagnetic phase are shown. Both components consist of 1000 atoms. Lower frame: The monopole mode frequency as a function of temperature in the limit of no interaction between components, clearly approaching $\sqrt{2}\omega_0$ for high temperatures.

frequency $2\omega_0$, where ω_0 is the trap frequency. While moving towards the paramagnetic-ferromagnetic phase, crossing this frequency increases to about $2.2\omega_0$. For higher temperatures all mode frequencies are shifted down and in the limit of $T \gtrsim T_F$ can be studied analytically.

To analyze small in-phase oscillations of a two-component interacting Fermi gas at the high-temperature limit we utilize the Madelung representation [41] of Eqs. (13). For the $+$ component this representation is expressed as a set of equations for the density and the velocity fields:

$$\begin{aligned} \frac{\partial n_+}{\partial t} + \nabla \cdot (n_+ \mathbf{v}_+) &= 0, \\ m \frac{\partial \mathbf{v}_+}{\partial t} + \nabla \left(k_B T \ln z_+ + V_{\text{tr}} + \frac{\delta V_{\text{int}}}{\delta n_+} + \frac{1}{2} m \mathbf{v}_+^2 \right) &= \mathbf{0}. \end{aligned} \quad (15)$$

At the high-temperature limit one has $n_+ \lambda^3 = f_{3/2}(z_+) \approx z_+$. Small oscillations are investigated by assuming small

deviations of the state from the equilibrium and by looking for periodic solutions for deviations. We write the density as $n_+ = n_{\text{eq}}^+ + \delta n_+$, where δn_+ is the departure from the equilibrium density and assume that both the velocity and δn_+ are small quantities. Since $n_{\text{eq}}^+ = \exp[(\mu_+ - V_{\text{tr}} - (\delta V_{\text{int}}/\delta n_+)_{\text{eq}})/k_B T]/\lambda^3$ and $\delta n_+ = \delta n_-$ (in-phase oscillations), Eqs. (15) are transformed to

$$\begin{aligned} \frac{\partial}{\partial t} \delta n_+ &= -\nabla \cdot (n_{\text{eq}}^+ \mathbf{v}_+), \\ m \frac{\partial \mathbf{v}_+}{\partial t} &= -\nabla \left[k_B T \frac{\delta n_+}{n_{\text{eq}}^+} + G(n_{\text{eq}}^+) \delta n_+ \right], \end{aligned} \quad (16)$$

where

$$G(n_{\text{eq}}^+) = \left[\left(\frac{\partial}{\partial n_+} + \frac{\partial}{\partial n_-} \right) \frac{\delta V_{\text{int}}}{\delta n_+} \right]_{n_+ = n_- = n_{\text{eq}}^+}, \quad (17)$$

and can be combined into a single equation for the density deviation

$$m \frac{\partial^2}{\partial t^2} \delta n_+ = \nabla \cdot \left[n_{\text{eq}}^+ \nabla \left(k_B T \frac{\delta n_+}{n_{\text{eq}}^+} + G(n_{\text{eq}}^+) \delta n_+ \right) \right]. \quad (18)$$

Now, the limit of small interactions can be analyzed. For weak interspecies interactions the second term on the right-hand side of Eq. (18) is neglected and $n_{\text{eq}}^+ = \exp[(\mu_+ - V_{\text{tr}})/k_B T]/\lambda^3$. Equation (18) can be rewritten as

$$m \frac{\partial^2}{\partial t^2} \left(\frac{\delta n_+}{n_{\text{eq}}^+} \right) = k_B T \nabla^2 \left(\frac{\delta n_+}{n_{\text{eq}}^+} \right) - (\nabla V_{\text{tr}}) \nabla \left(\frac{\delta n_+}{n_{\text{eq}}^+} \right). \quad (19)$$

The trapping potential is spherically symmetric, $V_{\text{tr}} = m \omega_0^2 r^2/2$, and we search for periodic solutions $\delta n_+/n_{\text{eq}}^+ \sim e^{-i\omega t}$ of Eq. (19) which are spherically symmetric as well. The solutions can be found by using the power series method. The lowest-energy mode has a frequency $\omega = \sqrt{2}\omega_0$, marked by a horizontal solid line in Fig. 3 (lower frame). The mode itself is $\delta n_+ \sim [1 - m\omega^2 r^2/(6k_B T)]n_{\text{eq}}^+$.

V. CONCLUSIONS

In summary, we have studied the dynamics of mixtures of repulsive Fermi gases consisting of a large number of atoms at nonzero temperatures. We find quantitative agreement with the experimental results of Ref. [38] on the spin-dipole oscillations. The calculations show the dependence of the critical repulsion $k_F a$ on the temperature. The transition to the ferromagnetic phase requires a larger value of $k_F a$ with increasing temperature, in agreement with Stoner's picture of itinerant ferromagnetism. We also model breathing modes of weakly interacting repulsive fermionic mixtures, getting agreement with the low-temperature results of Ref. [54] and showing a decrease of oscillation frequencies with an increase of temperature.

ACKNOWLEDGMENTS

The authors acknowledge support from the (Polish) National Science Center Grant No. 2018/29/B/ST2/01308. Parts of the results were obtained using computers at the Computer Center of University of Białystok.

- [1] B. DeMarco and D. S. Jin, *Science* **285**, 1703 (1999).
- [2] A. G. Truscott, K. E. Strecker, W. I. McAlexander, G. B. Partridge, and R. G. Hulet, *Science* **291**, 2570 (2001).
- [3] F. Schreck, L. Khaykovich, K. L. Corwin, G. Ferrari, T. Bourdel, J. Cubizolles, and C. Salomon, *Phys. Rev. Lett.* **87**, 080403 (2001).
- [4] S. R. Granade, M. E. Gehm, K. M. O'Hara, and J. E. Thomas, *Phys. Rev. Lett.* **88**, 120405 (2002).
- [5] Z. Hadzibabic, S. Gupta, C. A. Stan, C. H. Schunck, M. W. Zwierlein, K. Dieckmann, and W. Ketterle, *Phys. Rev. Lett.* **91**, 160401 (2003).
- [6] N. Navon, S. Nascimbène, F. Chevy, and C. Salomon, *Science* **328**, 729 (2010).
- [7] M. J. H. Ku, A. T. Sommer, L. W. Cheuk, and M. W. Zwierlein, *Science* **335**, 563 (2012).
- [8] C. Cao, E. Elliott, J. Joseph, H. Wu, J. Petricka, T. Schäfer, and J. E. Thomas, *Science* **331**, 58 (2011).
- [9] T. Rom, Th. Best, D. van Oosten, U. Schneider, S. Fölling, B. Paredes, and I. Bloch, *Nature (London)* **444**, 733 (2006).
- [10] D. Greif, T. Uehlinger, G. Jotzu, L. Tarruell, and T. Esslinger, *Science* **340**, 1307 (2013).
- [11] R. A. Hart, P. M. Duarte, T.-L. Yang, X. Liu, T. Paiva, E. Khatami, R. T. Scalettar, N. Trivedi, D. A. Huse, and R. G. Hulet, *Nature (London)* **519**, 211 (2015).
- [12] S. S. Kondov, W. R. McGehee, W. Xu, and B. DeMarco, *Phys. Rev. Lett.* **114**, 083002 (2015).
- [13] M. Schreiber, S. S. Hodgman, P. Bordia, H. P. Lüschen, M. H. Fischer, R. Vosk, E. Altman, U. Schneider, and I. Bloch, *Science* **349**, 842 (2015).
- [14] L. W. Cheuk, M. A. Nichols, K. R. Lawrence, M. Okan, H. Zhang, E. Khatami, N. Trivedi, T. Paiva, M. Rigol, and M. W. Zwierlein, *Science* **353**, 1260 (2016).
- [15] G. Salomon, J. Koepsell, J. Vijayan, T. A. Hilker, J. Nespolo, L. Pollet, I. Bloch, and C. Gross, *Nature (London)* **565**, 56 (2019).
- [16] C. S. Chiu, G. Ji, A. Bohrdt, M. Xu, M. Knap, E. Demler, F. Grusdt, M. Greiner, and D. Greif, *Science* **365**, 251 (2019).
- [17] M. Greiner, C. A. Regal, J. T. Stewart, and D. S. Jin, *Phys. Rev. Lett.* **94**, 110401 (2005).
- [18] C. Sanner, E. J. Su, W. Huang, A. Keshet, J. Gillen, and W. Ketterle, *Phys. Rev. Lett.* **108**, 240404 (2012).
- [19] A. Amico, F. Scazza, G. Valtolina, P. E. S. Tavares, W. Ketterle, M. Inguscio, G. Roati, and M. Zaccanti, *Phys. Rev. Lett.* **121**, 253602 (2018).
- [20] E. Vogt, M. Feld, B. Fröhlich, D. Pertot, M. Koschorreck, and M. Köhl, *Phys. Rev. Lett.* **108**, 070404 (2012).
- [21] M. Koschorreck, D. Pertot, E. Vogt, and M. Köhl, *Nat. Phys.* **9**, 405 (2013).
- [22] C. Luciuk, S. Smale, F. Böttcher, H. Sharum, B. A. Olsen, S. Trotzky, T. Enss, and J. H. Thywissen, *Phys. Rev. Lett.* **118**, 130405 (2017).
- [23] P. A. Murthy, N. Defenu, L. Bayha, M. Holten, P. M. Preiss, T. Enss, and S. Jochim, *Science* **365**, 268 (2019).
- [24] N. Luick, L. Sobirey, M. Bohlen, V. P. Singh, L. Mathey, T. Lompe, and H. Moritz, *Science* **369**, 89 (2020).
- [25] M. Bohlen, L. Sobirey, N. Luick, H. Biss, T. Enss, T. Lompe, and H. Moritz, *Phys. Rev. Lett.* **124**, 240403 (2020).
- [26] M. Lu, N. Q. Burdick, and B. L. Lev, *Phys. Rev. Lett.* **108**, 215301 (2012).
- [27] K. Aikawa, A. Frisch, M. Mark, S. Baier, R. Grimm, and F. Ferlaino, *Phys. Rev. Lett.* **112**, 010404 (2014).
- [28] A. Frisch, M. Mark, K. Aikawa, F. Ferlaino, J. L. Bohn, C. Makrides, A. Petrov, and S. Kotochigova, *Nature (London)* **507**, 475 (2014).
- [29] N. Q. Burdick, Y. Tang, and B. L. Lev, *Phys. Rev. X* **6**, 031022 (2016).
- [30] J. Kinast, S. L. Hemmer, M. E. Gehm, A. Turlapov, and J. E. Thomas, *Phys. Rev. Lett.* **92**, 150402 (2004).
- [31] M. W. Zwierlein, J. R. Abo-Shaeer, A. Schirotzek, C. H. Schunck, and W. Ketterle, *Nature (London)* **435**, 1047 (2005).
- [32] M. Bartenstein, A. Altmeyer, S. Riedl, S. Jochim, C. Chin, J. H. Denschlag, and R. Grimm, *Phys. Rev. Lett.* **92**, 203201 (2004).
- [33] A. Altmeyer, S. Riedl, C. Kohstall, M. J. Wright, R. Geursen, M. Bartenstein, C. Chin, J. H. Denschlag, and R. Grimm, *Phys. Rev. Lett.* **98**, 040401 (2007).
- [34] J. Joseph, B. Clancy, L. Luo, J. Kinast, A. Turlapov, and J. E. Thomas, *Phys. Rev. Lett.* **98**, 170401 (2007).
- [35] B. Clancy, L. Luo, and J. E. Thomas, *Phys. Rev. Lett.* **99**, 140401 (2007).
- [36] S. Riedl, E. R. Sánchez Guajardo, C. Kohstall, A. Altmeyer, M. J. Wright, J. H. Denschlag, R. Grimm, G. M. Bruun, and H. Smith, *Phys. Rev. A* **78**, 053609 (2008).
- [37] A. Sommer, M. Ku, G. Roati, and M. W. Zwierlein, *Nature (London)* **472**, 201 (2011).
- [38] G. Valtolina, F. Scazza, A. Amico, A. Burchianti, A. Recati, T. Enss, M. Inguscio, M. Zaccanti, and G. Roati, *Nat. Phys.* **13**, 704 (2017).
- [39] E. Stoner, *Philos. Mag.* **15**, 1018 (1933).
- [40] W. Kohn and L. J. Sham, *Phys. Rev.* **140**, A1133 (1965).
- [41] E. Madelung, *Z. Phys.* **40**, 322 (1927).
- [42] B. Kr. Dey and B. M. Deb, *Int. J. Quantum Chem.* **70**, 441 (1998).
- [43] A. Domsps, P.-G. Reinhard, and E. Suraud, *Phys. Rev. Lett.* **80**, 5520 (1998).
- [44] P. T. Grochowski, T. Karpiuk, M. Brewczyk, and K. Rzażewski, *Phys. Rev. Lett.* **119**, 215303 (2017).
- [45] P. A. M. Dirac, *Math. Proc. Camb. Philos. Soc.* **26**, 376 (1930).
- [46] F. Perrot, *Phys. Rev. A* **20**, 586 (1979).
- [47] K. Huang, *Statistical Mechanics* (Wiley, Hoboken, NJ, 2014).
- [48] K. Gawryluk, T. Karpiuk, M. Gajda, K. Rzażewski, and M. Brewczyk, *Int. J. Comput. Math.* **95**, 2143 (2018).
- [49] J. Ryszkiewicz, M. Brewczyk, and T. Karpiuk, *Phys. Rev. A* **101**, 013618 (2020).
- [50] J. von Stecher and C. H. Greene, *Phys. Rev. A* **75**, 022716 (2007).
- [51] A. Recati and S. Stringari, *Phys. Rev. Lett.* **106**, 080402 (2011).
- [52] W. Zwerger, *Science* **325**, 1507 (2009).
- [53] E. Lipparini, *Modern Many-Particle Physics* (World Scientific, Hackensack, NJ, 2003).
- [54] T. Karpiuk, P. T. Grochowski, M. Brewczyk, and K. Rzażewski, *SciPost Phys.* **8**, 66 (2020).
- [55] M.-I. Trappe, P. T. Grochowski, M. Brewczyk, and K. Rzażewski, *Phys. Rev. A* **93**, 023612 (2016).
- [56] M.-I. Trappe, P. T. Grochowski, J. H. Hue, T. Karpiuk, and K. Rzażewski, *New J. Phys.* **23**, 103042 (2021).